Rapid optical method for logging dust concentration *vs* depth in glacial ice

Predrag Miocinovic, P. Buford Price, and Ryan Bay

Physics Department, University of California, Berkeley, CA 94720

We describe a dust logger consisting of a downward-pointing phototube, 2 m below side-directed LEDs, attached to a cable that can lower the device down a 3-inch borehole filled with butyl acetate. LED photons that enter the ice are scattered or absorbed by dust grains, and those that reach the phototube provide a measure of dust concentration at a given depth. An increased dust concentration associated with an ancient colder climate will usually result in an *increase* in collected light, but may *decrease* collected light if air bubbles are present. The concept is based on six years of experience with pulsed light sources used to measure optical properties of deep Antarctic ice.

OCSI codes: 999.9999, 290.5850, 280.1100, 230.0040, 120.5820, 010.1100

1. Introduction

The dust logger described in this paper exploits some features of two modern optical techniques – the ocean transmissometer[1] and the AMANDA collaboration's method for mapping optical properties of deep glacial ice[2-5].

To study depth dependence of the mass concentration of particles (usually mainly microorganisms) in the ocean, oceanographers use a transmissometer, consisting of a 660 nm light-emitting diode (LED) viewed by a detector with an acceptance of ~1 degree at a distance of 25 cm on the axis of a cylinder through which water can freely flow. The transmission is corrected to standard conditions by simultaneously recording salinity, temperature, and density.

The contribution of yellowish dissolved organic matter is negligible at a wavelength of 660 nm. Beam attenuation due to pure seawater is taken to be constant and calibrated at the factory. Thus, the concentration of small particles, mostly microbial, is determined by subtracting the contribution of pure seawater to the attenuation by particles[6].

The AMANDA collaboration recently completed a huge observatory, buried in deep glacial ice, for tracking high-energy neutrinos from astronomical sources[7]. They used an optical method to determine at what depths the ice near the South Pole is sufficiently transparent to enable them to use the Cherenkov light from charged particles to determine the direction of the particles. Using a hot-water drilling technique, they melted cylindrical holes down to depths of ~2000 m in which were submerged strings of photomultiplier tubes (PMTs) and pulsed light sources, around which the water was allowed to refreeze. The PMTs served both to measure ice clarity as a function of depth and to record arrival times of Cherenkov light from relativistic charged particles. The light sources consisted of nitrogen lasers (337 nm) and LEDs (370 and 470 nm) at various depths in the ice and of light pulses transmitted from the surface down optical fibers to diffuser balls at various depths. Distances in solid ice between emitters and receivers were 10 to 120 m. From analyses of the distribution of arrival times of photons travelling between emitter and receiver, they were able to determine the wavelength dependence and depth dependence of both scattering coefficient and absorption coefficient for light as a function of depth in ice.

The AMANDA collaboration found that air bubbles dominated the light scattering at shallow depths, but that this contribution decreased with depth, due to compression of the bubbles and to their transformation into nearly invisible air hydrate crystals. At ~1400 m the transformation was complete. Below 1400 m the propagation of light was constrained only by the presence of dust particles deposited onto the snow by aerosols and later compacted into ice. The dust concentration inferred from the timing distributions and from application of Mie theory varied with depth in ice. Between 1400 and 2200 m near the South Pole the depth-dependence matched the pattern measured in the Vostok ice core at depths ~400 to ~930 m when properly scaled for differences in snow accumulation rate. The scaling was used to calibrate the age *vs* depth at South Pole[8] by using the age *vs* depth that had been determined by chemical and physical studies of the dust as a function of depth in the Vostok core[9].

In this paper we show that AMANDA's optical method of measuring dust concentration in glacial ice can be adapted to fit into a vertical cylinder slender enough to be lowered into a 3-inch access hole filled with butyl acetate, a standard drilling fluid. With this device, one can rapidly read out dust concentration at depths down to bedrock, measure scattering by air bubbles, measure dust in the presence of air bubbles, and detect volcanic ash layers with typical thickness ~1 cm. Advantages of this dust logger include speed, economy, and ability to measure both insoluble and soluble dust *in-situ* at ambient pressure.

2. Motivation for Dust Logging

Dust serves as a proxy for climate: it correlates well with δO^{18}, the oxygen isotopic composition. The δO^{18} in glacial ice and in planktonic foraminifera in sea sediments reflects the amount of the Earth's water frozen in ice. It is thus a measure of long-term variations of Earth's temperature – of great interest to paleoclimatologists[9]. In sea sediments the δO^{18} has traced a rough saw-tooth curve with a periodicity of close to 100,000 years for eight cycles, showing that major ice ages recur every 100,000 years[10]. For still earlier times the periodicity was roughly 41,000 years[11]. In both cases the periodicity is sufficiently precise that it must be controlled by astronomical phenomena. Some researchers believe in Milankovitch's explanation of the 10^5-year cycle in terms of changes in the eccentricity of the earth's orbit[10,11], while others argue that the gradual change in the earth's orbital inclination, which also has a period of 100,000 years, somehow causes the major ice ages[12]. The cause of the rather abrupt change from 41,000 to 100,000 years is unknown and is a subject of interest and speculation.

The paleoclimatic record in ice cores is not as extensive as in sea sediments. The analysis of the dust and δO^{18} in the oldest known ice core – at Vostok Station – shows that the deepest ice, at ~3500 m, has an age of ~420,000 years and that four cycles of ice ages are preserved[9], in accordance with the corresponding record in sea sediments. To make further progress in understanding the causes of ice ages, it would be highly desirable to have a portable dust logger that could search for major peaks in dust concentration as a function of depth in regions of Antarctica suspected of having ice much older than 420,000 years at its base.

A second motivation for a dust logger is in glaciology, especially in the study of the flow of very cold ice. To fully understand how ice flows, one needs to measure not only the stress and strain as a function of depth and position for ice flowing down an incline, but at the same time to determine the temperature, crystal fabric, chemical composition of impurities, and dust distribution in the same ice whose flow is being studied.

A third motivation is in volcanology, the aeolian transport of fine particles, and the possible role of volcanic ash in triggering world-wide cooling[13-15].

3. Design of a Compact Dust Logger

Figure 1 shows the design of a logger whose performance we have simulated. A high-speed mechanical access drill[16] would be used to drill a 3-inch diameter hole, to be filled with butyl acetate drilling fluid, extending from the surface down to bedrock. After removing the drill, the logger would be lowered on a cable kept taut by means of a weight, and readings would be taken either continuously or at predetermined depth increments. The cable (a standard four-connector logging cable) would provide power for LEDs and for a 1-inch downward-facing PMT and would return signals from the PMT to the surface.

We carried out simulations for light-emitting diodes (LEDs; Nichia Corporation) with peak emission at 370±10 nm; LEDs that emit at 470 nm would work just as well. An isotropic distribution of emitted photons was tracked from the light source into dusty ice, within which a small fraction of the photons scattered enough to impinge in an upward direction on a thin cylindrical disc of ice representing the PMT window. PMT and other electronic efficiencies were not simulated since we only wanted to find out relative changes in PMT signal as a function of dust or bubble concentration in a local region of the ice. Effective scattering coefficient, b_e, and absorption coefficient, a, were recalculated each time a photon passed into an ice layer (assumed to be horizontal) with a different dust or bubble concentration. To speed up the simulation, instead of a photon being absorbed, it was given a weight from 0 to 1, depending on the path traveled and type of ice traversed. At the detection volume, these weights were summed up as a probability of a given photon reaching that location in an upward direction. Due to cylindrical symmetry of the problem, we summed over all azimuth directions for photon emission and detection. Results were compared for photons emitted in 4 equal solid angle bins, from 0° (vertically upward) to 60°, 60° to 90°, 90° to 120°, and 120° to 180°.

Due to the similarity of refractive index of butyl acetate (n=1.390) to that of ice (n=1.322), we ignored refraction at the wall of the hole and treated butyl acetate as being equivalent to ice. Due to the small volume of butyl acetate relative to the volume of ice sampled by each photon, the resulting error is small. Measurements with a laboratory spectrophotometer showed that butyl acetate is quite transparent to light throughout the visible and UV down to a wavelength ≈ 260 nm.

The 2-m spacing between emitters and detector and the downward orientation of the PMT were chosen in order to reduce the fraction of photons that would scatter from the wall of the hole or from the drill fluid into the PMT without sampling much ice.

4. Results of Simulations

Dust bands without air bubbles. Inside a vertical band of enhanced dust concentration, the PMT signal as a function of time in response to a pulse of light from the LEDs showed a rapid rise to a peak value, typically occurring at a time ~5 ns after a hypothetical direct trajectory, followed by a roughly exponential decrease with time. The peak value of returned light, the integrated value for 1 to 50 ns, the integrated value for 1 to 100 ns, and the integrated value for 1 to 250 ns gave qualitatively the same result: all of them scale somewhat faster than linearly in dust concentration.

Figures 2 to 5 show examples of dust logger response characteristics and spatial resolution, with no bubbles present, for various vertical profiles with dust concentration rising to a maximum a factor six above background. This is conservative in that dust concentration increases as much as a factor 30 above background at glacial maxima, for example from the Holocene to the Last Glacial Maximum (LGM)[20]. In Fig. 2 the solid line shows a triangular dust profile, with background value normalized to unity. The three broken curves show the simulated PMT response integrated for 50, 100, and 250 ns for photons emitted at 60° to 90° zenith angles. The result is about the same for each of the three integration times: the signal sharply tracks the dust concentration, with a vertical resolution better than 1 m.

With integration time fixed at 100 ns, Fig. 3 shows the responses to a 4-m-deep region of enhanced dust concentration, for LEDs emitting in four different bands of zenith angle ranging from predominantly upward-directed to predominantly downward-directed. The best agreement in vertical location of the dust peak is obtained for LEDs emitting at 60° to 90°. The full width at half-maximum for the response of the dust logger is about the same as the thickness of the dust band, and the tail of the response is acceptably small.

Figure 4 shows the response to a sharply demarcated 20-m-thick dust band for three different integration times. Not surprisingly, the shortest integration time (50 ns) provides a response closest to the actual shape of the concentration profile. The spatial resolution is better than 1 m.

Figure 5 shows that the logger can resolve two 2-m-thick dust bands with a vertical separation of 10 m. Again, the 50-ns integration time gives the best spatial resolution.

In their optical study of dust at depths 1200 to 2300 m in South Pole ice, the AMANDA collaboration[18] detected bands of enhanced dust concentration typically at least 100 m thick and a factor 2 to 4 above minimum dust levels. Our simulations show that factor-of-two increases in dust concentration are easily detected by a dust logger.

Detectability of dust bands in regions of high bubble concentration. At a site where the accumulation rate is large, the record of the Holocene (the warm period from the present back to the end of the last ice age ~17,000 years ago) extends well below 1000 m, and the record of the LGM (~23,000 yr ago) peaks at a still greater depth, where all bubbles have undergone a phase transformation into solid air-hydrate crystals. However, at a site like Vostok or Dome C, snow accumulation rate is so low that the LGM record is at a depth of only a few hundred meters. At such a shallow depth, air bubbles contribute far more to light scattering than does dust, but they contribute nothing to absorption. We will now show that the dust logger can detect increases in dust concentration even at depths where bubbles dominate light scattering. In regions of strong scattering, a photon undergoes a random walk from emitter to receiver, and an analytic approximation is valid[17]:

$$u(d,t) = (3b_e(z)/4\pi v_g\, t)^{3/2} \exp\{-3d^2 b_e(z)/4v_g t - a(z)v_g t\} \qquad (1)$$

Here $b_e \equiv b_{bub} + b_{dust}$ is the sum of scattering coefficients for bubbles and dust; $v_g \equiv c/1.322$ is the group velocity of 370-nm photons in ice; t is the time after start of a light pulse; d = distance from emitter to receiver; and $a(z)$ is absorption coefficient of light (with dust but not bubbles contributing) at depth z. This equation, valid in the limit of many scatters ($d >> b_e^{-1}$), is much quicker to evaluate than running numerical simulations. The effective scattering coefficient for bubbles is given by

$$b_{bub} = (1 - \langle\cos\theta\rangle)\, n_{bub} \pi r_{bub}^2 \qquad (2)$$

where the first factor, with $\langle\cos\theta\rangle \approx 0.8$, takes into account the forward peaking in the scattering. For typical bubble concentrations and radii at depths of a few hundred meters ($n_{bub} \approx 500$ cm^{-3} and $r_{bub} \approx 100$ μm), $b_{bub} \approx 3$ m^{-1}. For a 2-m dust logger, the inequality $d >> b_e^{-1}$ is thus satisfied, even though $b_{dust} << b_{bub}$.

Figure 6 shows the surprising results of an application of eq. (1) to air bubbles + dust at a site with a very low accumulation rate. For b_{bub} we used eq. (2) with n_{bub} and r_{bub} taken from microscopic measurements of Vostok ice core samples[19], with values shown as solid circles. For b_{dust} representative of a warm period we chose a constant value of 0.025 m^{-1} and for dust representative of a cold period we chose a trapezoidal shape, ramping up linearly at depths from 300 to 400 m to a plateau value of 0.325 m^{-1} and decreasing back to 0.025 m^{-1} at depths from 475 m to 500 m. (This increase by a factor 13 is conservative in that increases by as much as a factor 30 are reported for glacial maxima.) The values used in our calculations are shown as solid squares. To illustrate the effect of the presence of bubbles on the dust signal it does not matter that we have ignored the subpeaks and valleys in the measured dust concentration in a cold period[20].

The solid curve shows the calculated signal in the dust logger for a 250-ns integration time. The surprising result is that, by virtue of their large scattering coefficient, the bubbles cause an amplified negative image of the dust band. In the absence of dust (dashed curve), the signal due to the bubbles would track the decline of b_b with depth; in the absence of bubbles, the signal due to the dust would *increase*, tracking the trapezoidal dust concentration (see Figs. 2 to 5 for triangular and square-wave patterns). When both bubbles and dust are present, the bubbles confine most of the photons to the dusty region until they are absorbed, thus leading to the negative image of the dust (solid curve).

Volcanic ash. To improve vertical resolution in locating a very thin band such as a cm-thick volcanic ash layer, the spacing between the PMT and the LEDs could be reduced to less than 1 m but more than the hole diameter, for example a 15-cm spacing. We modeled a volcanic ash band 1 cm thick and with a concentration and size distribution of ash chosen to mimic a typical ash band reported by Gow and Williamson[13]. The ratio of scattering coefficient to absorption coefficient was taken to be the same as that of the dust modeled in Figs. 2 to 5. The increased signal due to the ash band was detectable but located only to within the 1-m resolution of the 2-m logger. If the ash consisted of dark, highly absorbing grains, the amount of light reaching the phototube would be decreased instead of increased, thus providing a crude measure of composition.

It would be too time-consuming to scan the entire ~3-km-thick ice sheet at a resolution of a few cm. Instead, one could address specific questions in volcanology with a 15-cm logger after having established the approximate chronology at a drill site using the 2-m logger.

5. Conclusions

The principle on which the dust logger is based has been thoroughly demonstrated by the AMANDA collaboration, who used pulsed light emitters and phototube receivers separated at distances 10 to 120 m to map the vertical distribution of bubbles and dust. The same simulation techniques and diffusion equation used by AMANDA apply to our 2-m logger, which will be tested in the next Antarctic field season.

The logger can detect both thin and thick dust bands in bubble-free ice. It can also locate regions of large dust concentration even in the presence of a strongly scattering bubble concentration, but as a negative image, i.e., a decrease in signal superimposed on a high background signal due to bubbles alone. Because the refractive indices of the ice and of the butyl acetate are very similar, the results are insensitive to the scale of roughness of the hole. The logger is economical to build, and readout is continuous and straightforward. In contrast to methods such as laser light scattering and microscopic or chemical analysis, which require that a several-km-long core be removed from the ice, the logger can quickly read out data for *in-situ* ice at ambient pressure.

In the absence of bubbles, dust concentrations typical for glacial maxima produce very large signals; narrow dust bands only a few meters apart can clearly be resolved; and the signal tracks both triangular and square wave dust distributions to within ~1 m.

We thank M. Solarz and J. de la Torre for measuring light absorption in butyl acetate as a function of wavelength, and J. Keasling for the use of his spectrophotometer. This research was supported in part by National Science Foundation grant PHY-9971390.

References

1. For example, Wet Labs transmissometer (**http://www.wetlabs.com/Products/index.html**).

2. P. Askebjer *et al.*, "UV and optical light transmission properties in deep ice at the South Pole," Geophys. Res. Letters 24, 1355-1358 (1997).

3. The AMANDA collaboration, "Optical properties of deep ice at the South Pole: absorption," Appl. Optics 36, 4168-4180 (1997).

4. P. B. Price and L. Bergström, "Optical properties of deep ice at the South Pole: scattering," Appl. Optics **36**, 4181-4194 (1997).

5. Y. D. He and P. B. Price, "Remote sensing of dust in deep ice at the South Pole," J. Geophys. Res. **103** (D14) 17,041-17,056 (1998).

6. See, for example, S. P. Chung, W. D. Gardner, M. J. Richardson, I. D. Walsh, and M. R. Landry, "Beam attenuation and microorganisms: spatial and temporal variations in small particles along 140^{o}W during the 1992 JGOFS-EqPac transects," Deep-Sea Research Part II **43**, 1205-1211 (1996).

7. The AMANDA Collaboration, "The AMANDA neutrino telescope: principle of operation and first results," Astropart. Phys. **13**, 1-20 (2000); the AMANDA Collaboration, "Observation of high energy atmospheric neutrinos with AMANDA," submitted to Nature (2000).

8. P. B. Price, K. Woschnagg, and D. Chirkin, "Age *vs* depth of glacial ice at South Pole," Geophys. Res. Letters, in press (2000).

9. J. R. Petit *et al.*, "Climate and atmospheric history of the past 420,000 years from the Vostok ice core, Antarctica," Nature **399**, 429-436 (1999).

10. W. S. Broecker and J. van Donk, "Insolation changes, ice volumes, and the ^{18}O record in deep-sea cores," Geophys. Space Phys. **8**, 169-198 (1970).

11. J. Hays, J. Imbrie, and N. Shackleton, "Variations in the Earth's orbit: pacemaker of the ice ages", Science **194**, 1121-1132 (1976).

12. R. A. Muller and G. J. MacDonald, "Glacial cycles and astronomical forcing," Science **277**, 215-218 (1997); and "Spectrum of 100-kyr glacial cycle: orbital inclination, not eccentricity," Proc. Natl. Acad. Sci. USA **94**, 8329-8334 (1997).

13. A. J. Gow and T. Williamson, "Volcanic ash in the Antarctic ice sheet and its possible climatic implications", Earth Planet. Sci. Lett. **13**, 210-218 (1971).

14. E. Mosley-Thompson and L. G. Thompson, "Nine centuries of microparticle deposition at the South Pole", Quaternary Research **17,** 1-13 (1982).

15. G. A. Zielinski, "Use of paleo-records in determining variability within the volcanism-climate system", Quaternary Science Reviews **19**, 417-438 (2000).

16. B. Koci, G. Clow, and K. Cuffey. See http://area51.berkeley.edu/deepice2000/access.

17. P. Askebjer *et al.*, "Optical properties of the South Pole ice at depths between 0.8 and 1 kilometer," Science **267**, 1147-1150 (1995).

18. K. Woschnagg, for the AMANDA collaboration, "Optical properties of South Pole ice at depths from 140 to 2300 meters", *Proc. 26th International Cosmic Ray Conference*, August 17-25, 1999, Salt Lake City, Utah, pp. 200-203.

19. N. I. Barkov and V. Ya. Lipenkov, "Kolichestvennaya kharakteristika struktury l'da do glubiny 1400 m v rayone stantsii Vostok v Antarktide" [Numerical characteristics of ice structure down to a depth of 1400 m in the region of Vostok station], Mater. Glyatsiol. Issled. **51**, 178-186 (1984).

20. J. R. Petit, L. Mounier, J. Jouzel, Y. S. Korotkevich, V. I. Kotlyakov, and C. Lorius, "Palaeoclimatological and chronological implications of the Vostok core dust record", Nature **343**, 56-58 (1990).

Figure Captions

Fig. 1. Schematic design of the dust logger, immersed in a hole filled with transparent butyl acetate. Photons from side-directed LEDs scatter from dust or bubbles; some are absorbed by dust. Absorption by ice itself is negligible on a scale of tens of meters. A small fraction reaches the downward-directed phototube and provides a measure of dust or bubble concentration. Electronics are at the surface.

Fig. 2. Response of dust logger to a triangular distribution of dust in a 40 m thickness of bubble-free ice, for signal-integration times of 50, 100, and 250 ns, and for LEDs emitting at 60° to 90° zenith angles.

Fig. 3. Response to a thin dust band for LEDs emitting in four different angular intervals into bubble-free ice.

Fig. 4. Response to a dust band with constant concentration in 20 m of bubble-free ice.

Fig. 5. Response to two thin dust bands 2 m thick and 10 m apart in bubble-free ice.

Fig. 6. Response to bubbles + dust for 250 ns integration time. The scale on the left gives effective scattering coefficients calculated for microscopic measurements of bubble concentrations and radii in actual Vostok ice and for a trapezoidal distribution of dust above a constant low background dust level. The solid curve (arbitrary units) gives the response to the combination of bubbles + dust; the dashed curve shows the response if no dust were present. The dust, by absorbing some of the light, depresses the signal.

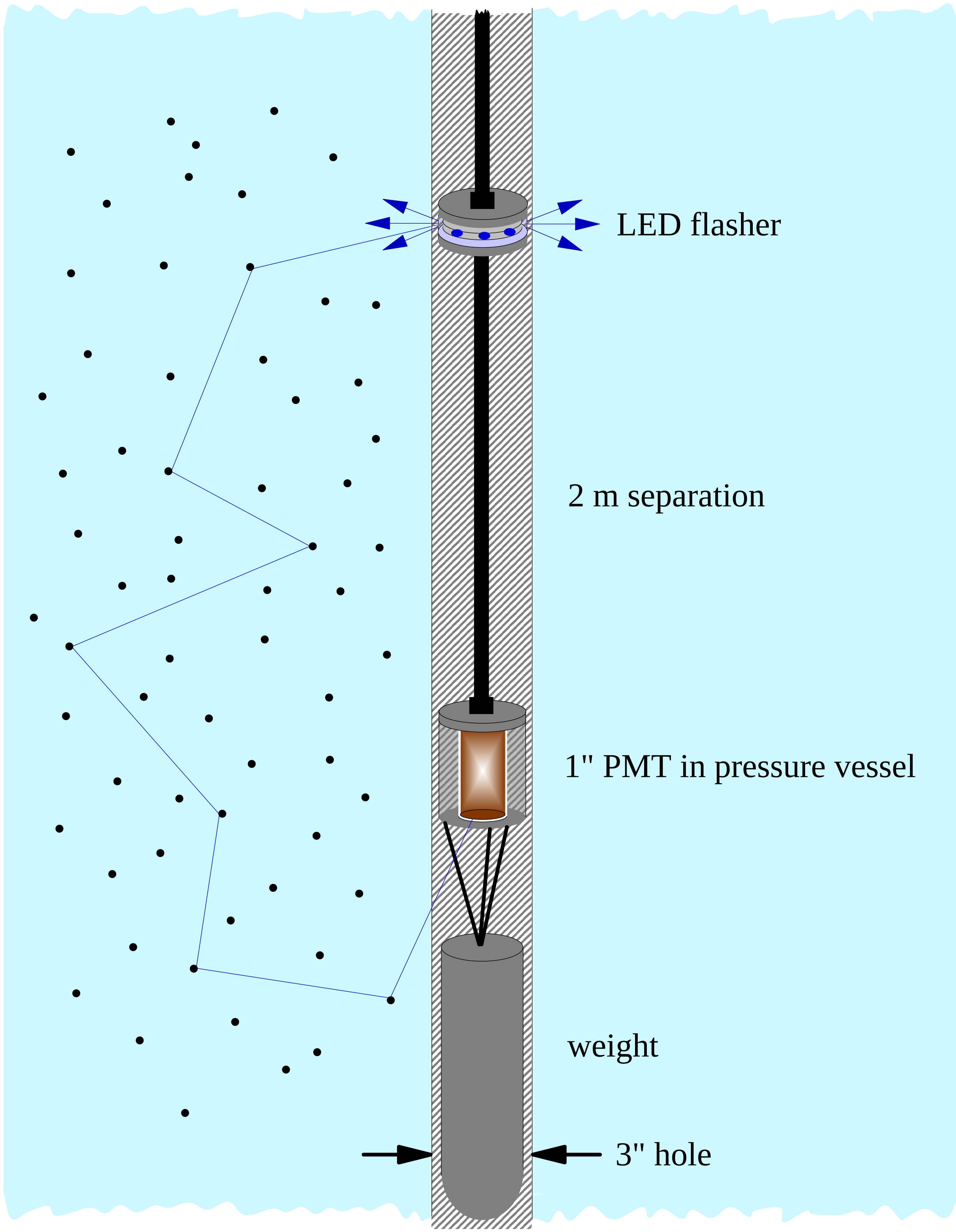
LED flasher
2 m separation
1" PMT in pressure vessel
weight
3" hole

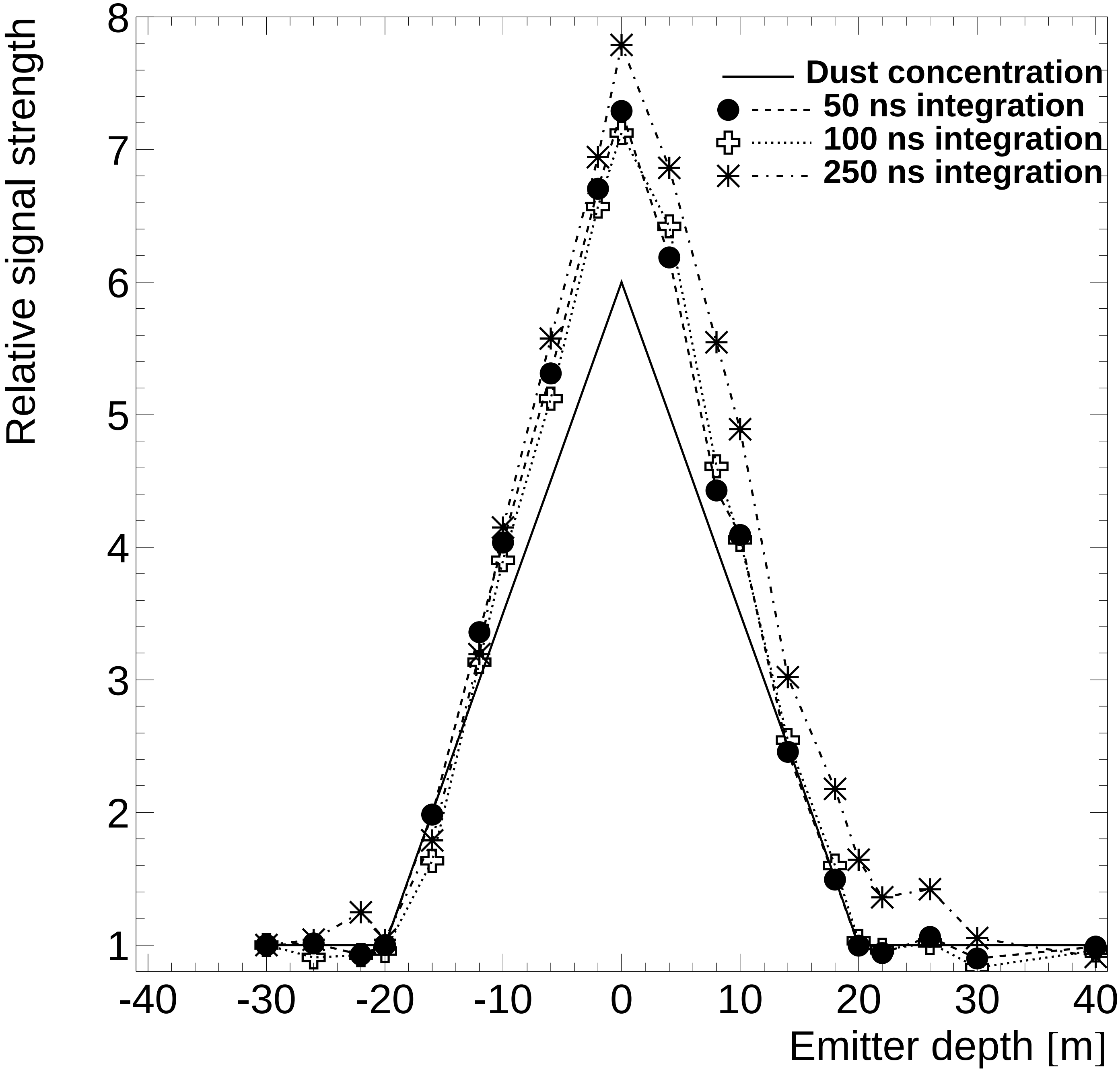

Relative signal strength
Emitter depth [m]
Dust concentration
50 ns integration
100 ns integration
250 ns integration

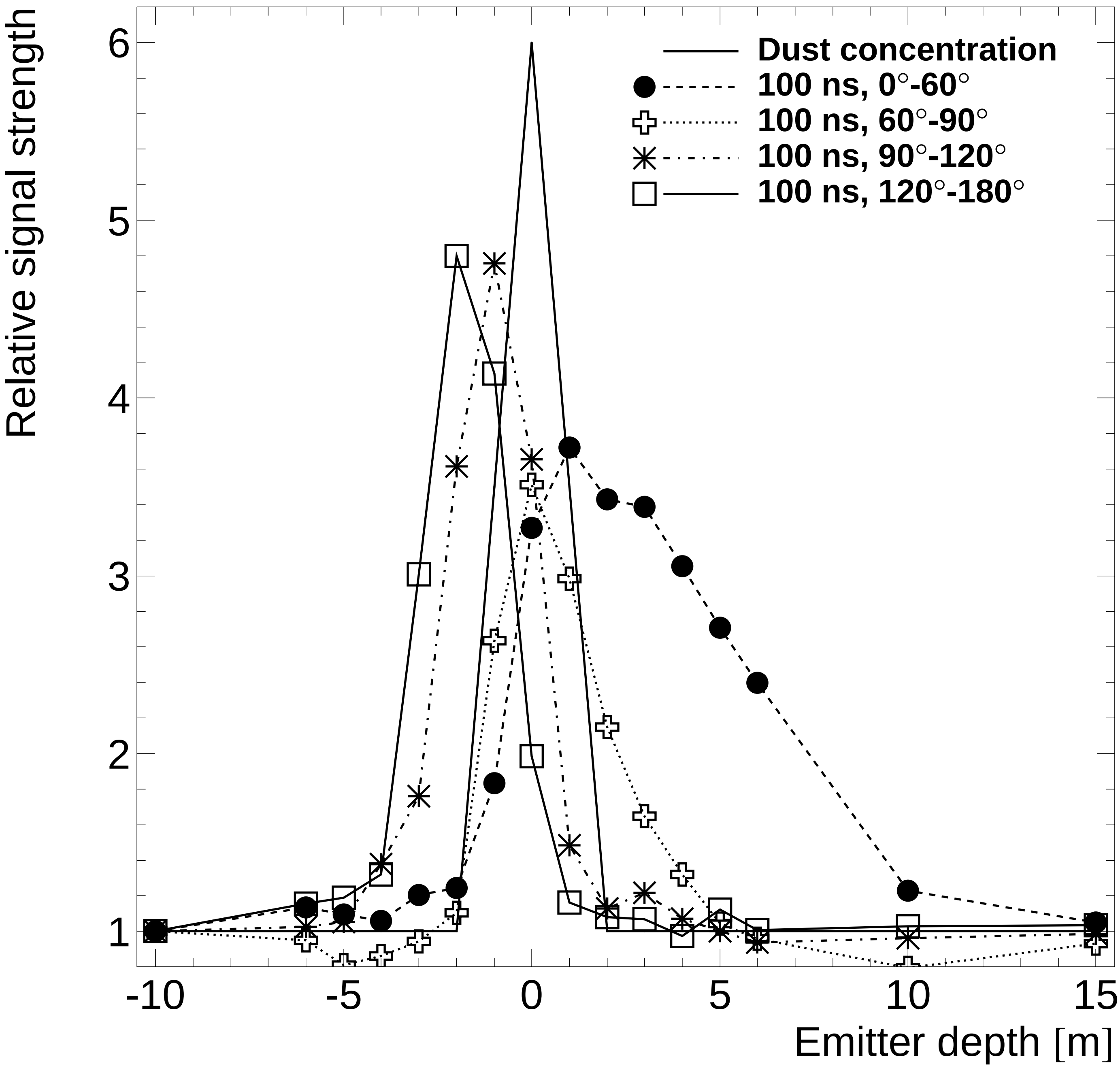
Relative signal strength
Emitter depth [m]
Dust concentration
100 ns, 0°-60°
100 ns, 60°-90°
100 ns, 90°-120°
100 ns, 120°-180°
6
5
4
3
2
1
-10
-5
0
5
10
15

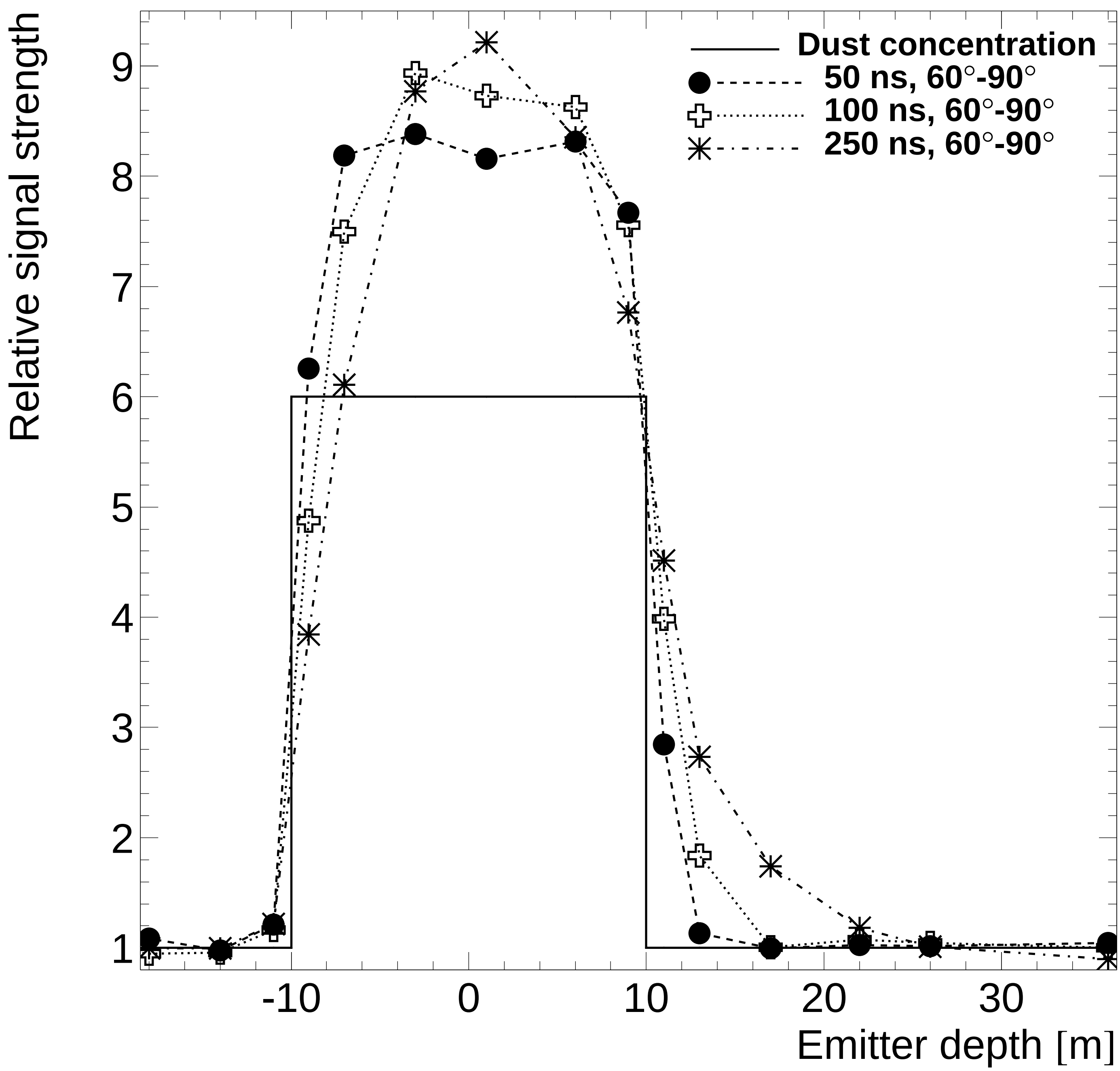
Dust concentration
50 ns, 60°-90°
100 ns, 60°-90°
250 ns, 60°-90°
Relative signal strength
Emitter depth [m]
1
2
3
4
5
6
7
8
9
-10
0
10
20
30

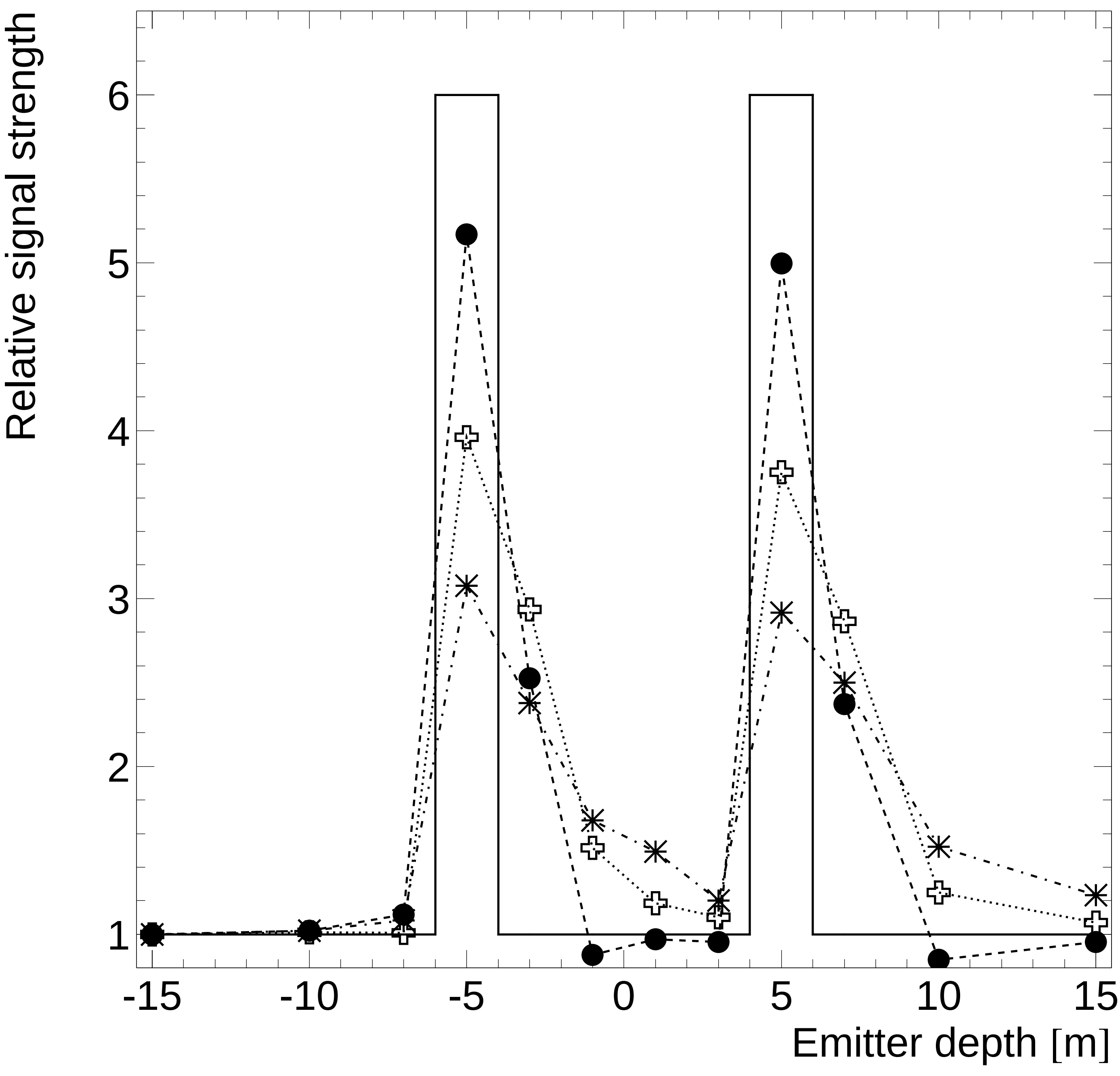

Relative signal strength
6
5
4
3
2
1
-15
-10
-5
0
5
10
15
Emitter depth [m]

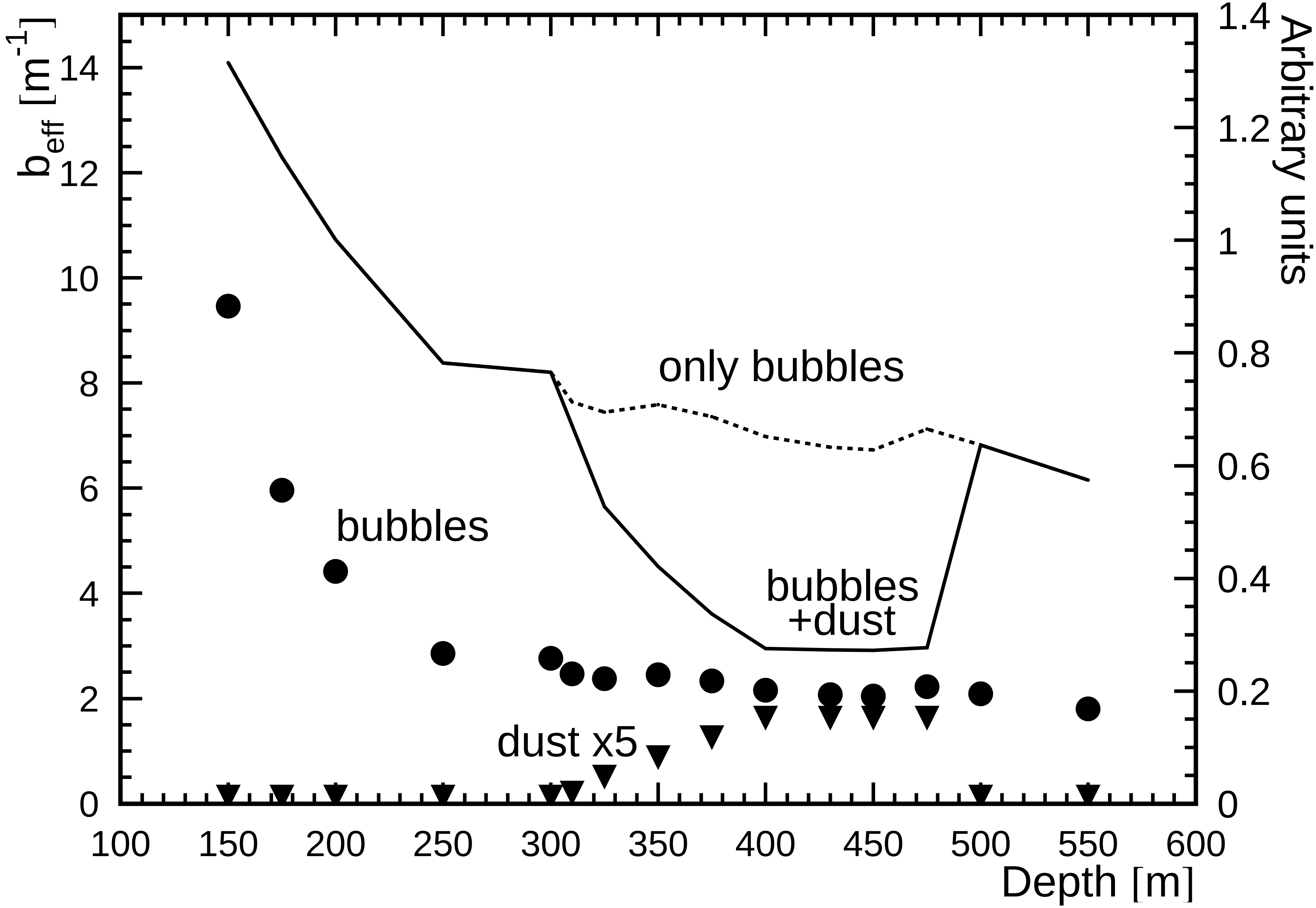

b_eff [m^-1]
Arbitrary units
only bubbles
bubbles
bubbles
+dust
dust x5
Depth [m]
0
2
4
6
8
10
12
14
0
0.2
0.4
0.6
0.8
1
1.2
1.4
100
150
200
250
300
350
400
450
500
550
600